SIMULATION OF CORE MELT POOL FORMATION IN A REACTOR PRESSURE VESSEL LOWER HEAD USING AN EFFECTIVE CONVECTIVITY MODEL

CHI-THANH TRAN* and TRUC-NAM DINH[1]
Nuclear Power Safety Division, Royal Institute of Technology
Roslagstullsbacken 21, Stockholm, Sweden, SE-106 91
[1] Present Address : Idaho National Laboratory, Idaho Falls, ID 83415, USA
*Corresponding author. E-mail : thanh@safety.sci.kth.se

Invited May 11, 2008
Received October 30, 2008

The present study is concerned with the extension of the Effective Convectivity Model (ECM) to the phase-change problem to simulate the dynamics of the melt pool formation in a Light Water Reactor (LWR) lower plenum during hypothetical severe accident progression. The ECM uses heat transfer characteristic velocities to describe turbulent natural convection of a melt pool. The simple approach of the ECM method allows implementing different models of the characteristic velocity in a mushy zone for non-eutectic mixtures. The Phase-change ECM (PECM) was examined using three models of the characteristic velocities in a mushy zone and its performance was compared. The PECM was validated using a dual-tier approach, namely validations against existing experimental data (the SIMECO experiment) and validations against results obtained from Computational Fluid Dynamics (CFD) simulations. The results predicted by the PECM implementing the linear dependency of mushy-zone characteristic velocity on fluid fraction are well agreed with the experimental correlation and CFD simulation results. The PECM was applied to simulation of melt pool formation heat transfer in a Pressurized Water Reactor (PWR) and Boiling Water Reactor (BWR) lower plenum. The study suggests that the PECM is an adequate and effective tool to compute the dynamics of core melt pool formation.

KEYWORDS : Heat Transfer, Effective Convectivity Model, Characteristic Velocity, Phase Change, Mushy Zone, Core Melt Pool, Severe Accident

1. INTRODUCTION

In a hypothetical severe accident, it is possible that the molten corium will be relocated into the lower plenum of the Reactor Pressure Vessel (RPV) [1]. In the presence of water pool in the lower plenum during the relocation, the core melt is fragmented and quenched, forming a debris bed (or a debris cake). It is probable that after the bed dryout, the debris is heated up again and a molten corium pool is formed in the lower plenum. The behavior and heat transfer regime of the so-formed melt pool directly affect thermal loads imposed on the reactor internal structures and vessel wall, defining the RPV failure's modes and timing.

Numerical analysis of melt pool behavior in the lower plenum, especially in a BWR, is a challenge for CFD simulations due to large dimensions, complex flow in complex 3D geometry and long term transient of the accident progression [2]. On the one hand, the BWR lower plenum contains a forest of Control Rod Guide Tubes (CRGTs) which make the geometry and flow complex. On the other hand the coolant flow through CRGTs can be used to remove the decay heat during an accident, thus serving as a Severe Accident Management (SAM) mitigative measure. To simulate transient heat transfer of a core melt pool formed in the BWR lower plenum, methods of CFD, neither with turbulence models nor Direct Numerical Simulation (DNS) can be applied due to their computational expense. At the same time, such lumped-parameter methods as used in severe accident codes [3,4] do not provide the needed capability to examine delicate effects of the flow in the cooling configuration of lower plenum geometry. The objective of the present work is to develop a simulation tool that enables a mechanistic analysis of core melt pool formation heat transfer and melt-vessel interactions in the LWR lower plenum.

The technical approach adopted in the present paper is built on our recent development [5], in which we advanced the concept of the Effective Convectivity Model (ECM). In fact, the ECM is built on the Effective-Conductivity-Convectivity Model (ECCM) first developed in [6]. The resulting code MVITA was validated and applied to PWRs [1]. Notably, the ECCM method uses correlation-based characteristic velocities to convect the heat to pool

boundaries in addition to the effective diffusivity [7]. In [5], we showed that the modified formulation of effective convectivity alone is capable of providing accurate simulations of turbulent natural convection heat transfer in a volumetrically heated liquid pool. Furthermore, to overcome 2D and other limitations of the MVITA code, the ECM method was implemented in **Fluent** CFD code [8], to take the advantages of the **Fluent** pre- and post-processing, its 3D solver for heat transfer in complex geometries.

In the present paper, we extend the ECM method to phase-change problems, to enable simulations of core melt pool formation in the lower plenum. The resulting method is named the Phase-change ECM (the PECM). In the rest of this section, we review the previous developments of relevance to the subsequent discussion of the PECM. Section 2 gives the PECM basic assumptions and descriptions. In Section 3, the PECM performance is examined, followed by recommendations on the model. Section 4 presents analysis results using the PECM and discusses the method applicability for simulations of realistic accident progression in a BWR lower plenum. Concluding remarks are presented in Section 5.

1.1 Experimental Studies

While early studies of melt pool convection were conducted with isothermal boundary conditions without phase change, during the 1990s and early 2000s, several experimental programs were performed with phase change, ranging from real corium tests (RASPLAV, MASCA) [9,10], to simulant salt tests (RASPLAV-SALT, SIMECO, LIVE) [11-13] and tests using water as the corium simulant (COPO II, BALI) [14,15].

The main objective of the RASPLAV Project was to study corium melt pool convection in conjunction with the chemical processes in the debris bed/molten pool and at the interface boundaries. The RASPLAV experiments showed that the corium melt pool convection flow field may be similar to those that prevail, at equivalent *Ra* numbers, in facilities employing simulant materials. The salt and real material tests confirmed that heat transfer correlations established in simulant materials tests can be used for the convection of homogenous corium melt pool at equivalent *Ra* numbers [9].

The SIMECO experiment was performed to investigate the effect of boundary crusts and mushy layers on natural convection heat transfer. The experiment showed that the upward Nusselt number is close to that determined from the Steinberner-Reineke correlation [12]. More recently, to address remaining uncertainties in melt pool heat transfer with phase change, the LIVE program was initiated at Forschungszentrum Karlsruhe (FzK). The LIVE experimental program is in its active phase and analysis of LIVE data is in progress.

The COPO II and BALI experiments were performed in large 2D slice geometry to study the thermal-hydraulics of a corium pool, the simulant used was water. The boundaries of the pool were cooled till freezing so truly isothermal boundaries were established. The measured values of the COPO II showed that the upward Nusselt numbers are consistent with BALI results. However, they are slightly higher than predicted by the widely used correlation of Steinberner and Reineke, and also higher than measured in 3D ACOPO experiments which did not have crusts at the boundaries. For the side and bottom boundaries, the COPO II and BALI experiments showed clearly higher heat transfer coefficients (20-30%) than those in the ACOPO and those predicted by the Steinberner-Reineke correlation, particularly regarding the vertical boundary [14,15]. The reason for this discrepancy may be the effect of water density reversal at 4°C on heat transfer of the pool. The other potential reason is the ice crust surface roughness which intensifies turbulence mixing of the pool, particularly along the boundary layers. The third reason is that in the COPO II and BALI experiments, the pool boundaries are frozen, causing a large temperature difference between the pool boundary and the bulk of the fluid. Therefore the fluid properties are non-uniform, raising a question of the reference temperature at which the fluid properties are applied in the heat transfer correlations.

Nevertheless, a unifying trend derived from the experimental studies is that the experimental heat transfer correlations built on data from simulant fluid experiments under isothermal boundary conditions are applicable to a melt pool with phase change.

1.2 Numerical Studies

The numerical methods used for solving phase-change problems can be divided into two main groups. The first group is named strong numerical solutions [16,17]. In this group the focus is on implementing finite-difference and finite-element techniques to the strong formulation of the process, locating fronts and finding temperature distributions at each time step or employing a transformed coordinate system to immobilize the moving interface. The second group is named weak numerical solutions, an example is presented in [18]. In the second group, a popular approach used for the numerical modeling of phase-change systems is so called the "fixed" grid method. Examples of fixed grid solutions of convection-diffusion phase change can be found in [19] and [20].

The most important and widely used numerical method to solve phase-change problems is the enthalpy formulation. This approach does not trace the exact position of the phase-change interface, thus allowing the method to be formulated in a fixed region, and no modification of the numerical scheme is necessary in order to satisfy the conditions at the moving phase-change interface. Furthermore, this method is suitable both for the problems where the phase change occurs at a single temperature and where the phase change occurs over a temperature range [20].

The major problem of the enthalpy formulation in a fixed grid is in accounting for the zero velocity condition as liquid turns to solid. To overcome this difficulty, a subtle approach in making the viscosity a function of the latent heat was developed [19]. Computational cells in which phase change is occurring are modeled as pseudo porous media with the porosity, so the method was called the enthalpy-porosity technique. The functional relationship of the latent heat is a linear porosity dependency. The method was widely used for modeling the phase-change mushy zone, and was tested with experiments [21,22]. This method was also implemented in **Fluent** code [8] to model the solidification/melting process.

2. PHASE-CHANGE EFFECTIVE CONVECTIVITY MODEL METHOD

2.1 Phase-change Modeling

In the present work, the enthalpy formulation is used to model the solidification/melting process. The enthalpy formulation is based on the assumption of total enthalpy as a dependent variable, along with the temperature. According to the enthalpy formulation, the phase-change material is assumed to be mushy for temperature T in the mushy zone:

$$T_{SOL} \le T \le T_{LIQ} \tag{1}$$

Assuming that the viscous dissipation is neglected, from a single enthalpy conservation equation which is common for solid, mushy and liquid regions, the flowing equation can be derived:

$$\frac{\partial}{\partial t}(\rho C_p T) = \nabla \bullet (k \nabla T) - \frac{\partial(\rho \Delta H)}{\partial t} + S_c \tag{2}$$

where S_c is the modified source term which includes the convective terms and material volumetric heat source. We can separate two types of a mushy zone: a mushy zone in which the solid is fully dispersed in the liquid phase, and a fixed columnar zone [23]. The mushy zone of core melt is characterized by dendrite structure which is similar to a columnar zone. In the PECM, the fixed columnar zone model is considered, the modified source term S_c is defined as follows:

$$S_c = -\nabla \bullet (\rho u C_p T) - \nabla \bullet (\rho u L) + Q_v \tag{3}$$

In this fixed columnar zone, however, the solid flow is zero, and no net latent heat is convected. As a result, the second convective term of equation (3) is zero. Thus there are two mechanisms of heat transfer within a mushy zone: the conduction and convection of the liquid fraction. The convection is possible only within the liquid fraction.

The latent heat of fusion ΔH is constrained by the limits:

$$0 \le \Delta H \le L \tag{4}$$

or

$$\Delta H = F_L \times L \tag{5}$$

where F_L is the local liquid fraction. A key feature in the development of the fixed grid method is the definition of the local liquid volume fraction F_L. In general, the local liquid fraction in the mushy zone depends on the nature of solidification. The local liquid fraction could be a function of temperature, cooling rate, solidification rate and the local liquid fraction field, i.e. the mushy zone structure. A general form of the local liquid fraction versus temperature function is non-linear (Fig. 1). In this figure, the step change at the solidus temperature (solid-mushy interface) can be associated with a eutectic phase change, and the step change at the liquidus temperature (mushy-liquid interface) can be used to approximately represent a kinetic under-cooling at the dendrite tips [24].

In many systems, it is reasonable to assume that the liquid fraction is a function of temperature alone. In the **Fluent** the local liquid fraction in a mushy zone of non-eutectic mixture is defined as follows [8]:

$$F_L = \frac{T - T_{SOL}}{T_{LIQ} - T_{SOL}} \text{ where } T_{SOL} < T < T_{LIQ} \tag{6}$$

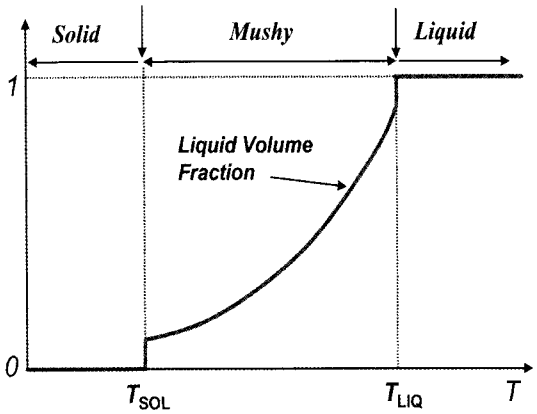

Fig. 1. A General Liquid Fraction-temperature Curve

However, direct using equation (6) to update the liquid fraction usually results in poor convergence of the energy equation. Thus, the method suggested by Voller and Swaminathan [25] is used to update the liquid fraction. For pure metals, a method based on specific heat [19] is used instead. In the PECM, based on the updated temperature, the liquid fraction described in (6) is used to determine the heat transfer characteristic velocity in a mushy zone (subsection 2.3).

2.2 ECM Method

The ECM approach is developed based on the insights gained from the CFD study to enable sufficiently-accurate simulations of melt pool heat transfer in a BWR lower plenum in a computationally effective manner. Detailed descriptions of the ECM method are reported in [5]. A short introduction to the ECM method is provided here.

In the ECM method we do not solve Navier-Stokes equations, only energy conservation equation (2) is solved using the **Fluent** solver. The convective terms are included in the equation to describe turbulent natural convection heat transfer. Instead of involving the instantaneous fluid velocity u, the directional heat transfer characteristic velocities $U_{x,y,z}$ are implemented in the modified heat source S_c.

The characteristic velocities (denoted as U_{up}, U_{down} and U_{side}) are derived using energy balance equations, and presented through heat transfer coefficients as follows:

$$U_{up} = \frac{\alpha}{H_{pool}} \times \left(Nu_{up} - \frac{H_{pool}}{H_{up}} \right) \tag{7}$$

$$U_{side} = \frac{\alpha}{H_{pool}} \times \left(Nu_{side} - \frac{2 \times H_{pool}}{W_{pool}} \right) \tag{8}$$

$$U_{down} = \frac{\alpha}{H_{pool}} \times \left(Nu_{down} - \frac{H_{pool}}{H_{down}} \right) \tag{9}$$

where H_{pool} is the height of the melt pool, H_{up} is the height of the pool upper mixed region; H_{down} is the height of the lower stratified region; W_{pool} is the pool width. The H_{pool} and W_{pool} are taken from the transient values of the formed pool during the simulation, H_{up} (and H_{down}) is assumed to be as follows:

$$H_{up} = \frac{H_{pool} \times Nu_{up}}{Nu_{up} + Nu_{side} + Nu_{down}} \tag{10}$$

Due to long transient behavior, melt pool formation progression can be assessed as a quasi steady state. This assumption allows us to apply heat transfer correlations obtained in a simulant fluid experiment under isothermal boundary conditions in the ECM and the PECM for phase-change simulations. In the present study, the average Steinberner-Reineke correlations for upward, sideward and downward Nusselt numbers [26] are implemented. The reason is that in the melt pool formation process, the configuration of interest has three cooled walls: the top, bottom and side (i.e. CRGT and vessel) walls, and Steinberner-Reineke experiments provided a full set of correlations of heat transfer for these three walls. The Steinberner-Reineke correlations were obtained at a higher Rayleigh number range approaching that of the prototypic reactor conditions. Despite aforementioned slight discrepancies with the COPO II and BALI experiments, validity of these correlations was confirmed in the other experiments, namely the COPO and ACOPO experiments [27,28], and the phase-change SIMECO experiment [12].

To describe the sideward heat transfer coefficient profile due to the boundary layer development along an inclined cooled surface, the Eckert-type correlation [29] is used:

$$Nu_{side} = 0.508 \, \mathrm{Pr}^{1/4} \left(\frac{20}{21} + \mathrm{Pr} \right)^{-1/4} Ra_y^{1/4} \tag{11}$$

The characteristic velocities are implemented in the **Fluent** using User Defined Function (UDF). It is seen from equation (3) that the convective terms of the characteristic velocities are added only into the cells where temperature gradients are available. During the simulation, temperature gradients can be obtained from the cell variables in each time step, so adding the artificial convective terms to the heat source S_c is then possible in the next time step. The added heat must be extracted from the whole pool domain to ensure energy balance.

2.3 Fluid Velocity and Characteristic Velocity in a Mushy Zone

It is seen from (3) that to solve the heat equation, it is necessary to define the fluid velocity in the mushy zone. The fluid velocity in a mushy zone defines heat transfer characteristics of the mushy zone and may have a certain influence on the dynamics of the melting/solidification front and change the behavior of melt pool formation.

We name the fluid velocity in a mushy zone the mushy-zone velocity (or the mushy velocity). In the CFD method, there are two approaches of resolving the mushy velocity: the first is a determination via the permeability of the mushy zone and the second is a determination via mushy-zone viscosity.

The first approach assumes that the dendrite mushy zone can be considered as a porous media, the permeability

of which is a function of the porosity λ (or liquid fraction $\lambda=1-F_S=F_L$) [19]. At the solid interface, the liquid fraction is close to zero and permeability reaches zero, while in the region with liquid fraction approaching unity, the permeability reaches the infinitive and the effective velocity of the fluid should be equal to the actual liquid velocity u_{LIQ}. Consequently, in the enthalpy formulation, the mushy region is considered as a columnar zone, the mushy velocity is governed by the Darcy law and the superficial velocity (the ensemble-average velocity) in a mushy zone is defined through liquid fraction F_L as follows:

$$u = u_{LIQ} \times F_L \tag{12}$$

The second approach assumes that the mushy velocity depends on mushy-zone viscosity. Corium viscosity can be modeled as suspension viscosity which may be a linear or exponential function of the solid fraction F_S. For high-concentration suspensions, a higher-order term than F_S^2 solid fraction dependency of viscosity may be required [30].

In the PECM, we implement only the heat transfer characteristic velocity (or simply called characteristic velocity). To support the PECM, several approaches to model the characteristic velocity in a mushy zone were investigated. One may assume that the mushy-zone velocity depends on liquid fraction, which can further be related to temperature of the binary mixture in a mushy zone by either linear, linear-eutectic, Scheil, or power-law relationship [25]. Large uncertainties remain regarding such dependencies, which are a subject in our future investigations. On physical basis, the fluid velocity in the mushy region is expected to decrease gradually until it reaches the solid interface. In one scenario, the fluid velocity decreases rapidly when it enters into the mushy region and decreases slowly when it gets closer to the solid interface. In another scenario, the fluid convection may stiffen or even stagnate as it goes deeper into the dendrite zone. To examine the effect of fluid mushy velocity on phase-change heat transfer, three descriptions of mushy characteristic velocity are then implemented using linear, quadratic and n-order dependencies on liquid fraction. These dependencies are expressed as follows:

$$U_{mushy} = U_{x,y,x} \times F_L \tag{13}$$

$$U_{mushy} = U_{x,y,x} \times F_L^2 \tag{14}$$

$$U_{mushy} = U_{x,y,x} \times F_L^n \tag{15}$$

where U_{mushy}, $U_{x,y,z}$ are the characteristic velocities in the mushy zone and bulk fluid.

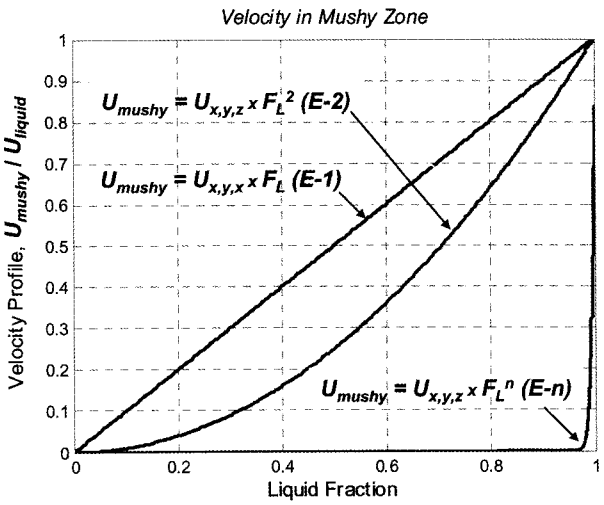

Fig. 2. Three Mushy-zone Characteristic Velocity Models

We denote the case of linear dependency, equation (13) as E-1, the case of quadratic dependency, equation (14) as E-2, and the case of equation (15) as E-n (no mushy characteristic velocity or n-order dependency function, $n\rightarrow\infty$). Liquid fraction dependency of mushy characteristic velocity is shown in Fig. 2. Results of PECM simulations for different mushy characteristic velocity models will be compared with those of CFD simulations.

3. VALIDATION

Due to lack of direct experimental data and correlations on phase-change heat transfer under relevant conditions, a dual approach is employed to examine the performance and provide validation for the PECM. The first approach is validation against the existing experimental data or correlations wherever available, and the second is to compare PECM simulations with results obtained by CFD simulations performed for the same geometry and conditions.

To ensure the accuracy of a complex flow simulation, Adaptive Mesh Refinement (AMR) technique of **Fluent** is used. The AMR tool of **Fluent** creates a high-resolution mesh based on the gradient of liquid/solid fraction. A high-resolution mesh is provided in the phase-change interface of the solid debris and liquid melt to resolve the melting front.

3.1 Fluid Layer Cooled from the Top

The purpose of this simulation task is to examine the consistency of the CFD and PECM simulations with different mushy characteristic velocity models, comparing

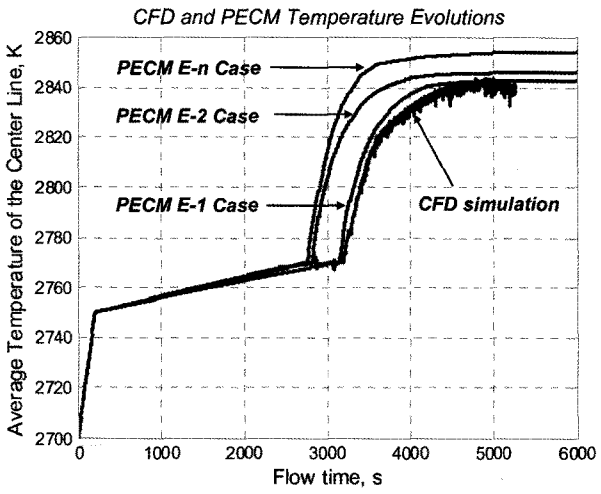

Fig. 3. CFD and PECM Predicted Transient Pool Centerline Temperature of the Fluid Layer Cooled from the Top

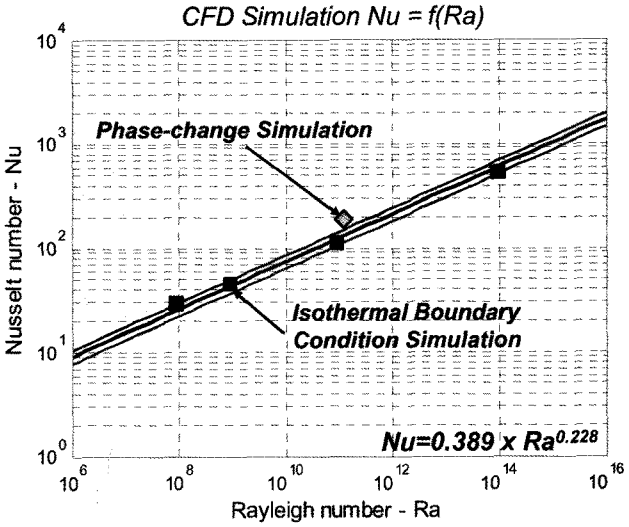

Fig. 4. Kulacki-Emara Correlation and CFD Simulation Heat Transfer Coefficients

Table 1. Fluid Layer Characteristics and Heat Transfer Coefficients Computed by the CFD and PECM Methods

Items	Reference temperature T_{SOL} (ΔT=T-T_{SOL})	Reference temperature T_{MP} (ΔT=T-T_{MP})	Reference temperature T_{LIQ} (ΔT=T-T_{LIQ})
Rayleigh number	1.47×10^{11}		
Fluid layer height	0.199		
Kulacki-Emara correlation Nusselt number	136.9		
	CFD simulation (with phase change)		
Temperature difference, K	87.8	78.9	68.9
Nusselt number	147.3	163.9	187.7
	CFD simulation (without phase change)		
Temperature difference, K	88.8		
Nusselt number	145.8		
	PECM simulation (**E-1** case)		
Temperature difference, K	88.5	78.9	69.7
Nusselt number	149.4	167.6	189.7

heat transfer coefficients of the phase-change case with that predicted by the experimental correlation (Kulacki-Emara correlation, [31]).

A small box full of internally heated corium is cooled from the top wall. Solidus and liquidus temperatures (T_{SOL} and T_{LIQ}) applied in the CFD and PECM simulations are 2750 K and 2770 K, respectively. The domain's initial temperature is 50 K lower than solidus temperature.

As a baseline benchmark, we use the CFD method to compute fluid flow and heat transfer of the fluid layer. The cooled wall is kept at temperature lower than solidus temperature, so a truly isothermal boundary condition, i.e. with the phase-change boundary, is achieved. A fine nodalization was applied to effectively provide Large-Eddy Simulations (LES) of turbulent natural convection in fluid layer without invoking an explicit Sub-Grid Scale (SGS) turbulence model [32]. Solutions obtained in the CFD simulations are grid-resolution independent.

The results of simulations show good agreement between the temperature evolutions computed by the CFD

and by the PECM method (Fig. 3). The linear dependency of mushy characteristic velocity on fluid fraction provides the most consistent result with the CFD prediction. The other mushy characteristic velocity models give slightly higher pool temperature. Table 1 shows good agreement of the heat transfer coefficients predicted by the CFD and PECM simulations with the linear liquid fraction dependency of mushy characteristic velocity (E-1).

Results of the CFD simulations of fluid layer cooled from the top without phase change (the boundary temperature is the liquidus temperature) are well agreed with the correlation in a wide range of Rayleigh number (Fig. 4). However, the results of the CFD simulation with phase change exhibit an uncertainty in determining the heat transfer coefficient. Applying solidus reference temperature T_{SOL}, the calculation gives a slightly higher Nusselt number compared with the result predicted by the correlation. In the case of applying liquidus reference temperature T_{LIQ} the Nusselt number appears to be 37% higher than that predicted by the correlation (Table 1). It suggests a choice of a reference temperature T_{REF} which is higher than T_{SOL} and lower than T_{LIQ}. For the linear dependency mushy characteristic velocity, it is recommended to apply the reference temperature in between T_{SOL} and T_{LIQ} (i.e. midpoint T_{MP}), although for the fluid layer case under consideration this temperature still gives a deviation of about 20% compared with the correlation, and 12% with the CFD simulation result without phase change.

An additional CFD simulation performed with a eutectic mixture (T_{SOL}=T_{LIQ}) shows a closer result of Nusselt number compared with the Kulacki-Emara correlation. The deviation between the two heat transfer coefficients is about 14% which is acceptable. However, the reason of deviation may be explained. A detailed examination view of the interface shows that the phase-change boundary is unsmooth. It is argued that due to the pool surface roughness, the actual liquid-solid interface area is enhanced. Such an increase of the heat transfer area provides additional heat removal capacity, increasing the effective heat transfer coefficient (calculated for a smoothed surface area).

Otherwise, we assume that the deviation under question is due to the phase-change effect as it was observed experimentally [14,15]. It is also possible that the deviation is due to numerical errors which are related to isothermal phase-change interface treatment of the numerical scheme [19] implemented in the **Fluent** for eutectic mixtures. Resolution of this issue is beyond the subject of the present study and envisioned as a topic of future work.

3.2 Scaled PWR Lower Plenum Simulation

The second test case considered is a scaled 2D model of PWR lower plenum represented by a semicircular section with the radius of 200 mm. The material used is the corium with the volumetric heat rate of 1.5 MW/m^3. The pool Rayleigh number reaches $Ra = 4.8 \times 10^{11}$.

The purpose of the simulation is to examine the mushy-zone characteristic velocity models, to check consistency of the PECM and CFD simulations, and predict melt pool energy splitting.

The boundary conditions applied to the top and vessel walls are isothermal with temperature of 100 K lower than solidus temperature of the core material. The solidus and liquidus temperatures are 2750 K and 2800 K, respectively. It is expected that a thin crust will be formed along the pool boundaries. To compare heat transfer coefficients and energy splitting, we also perform CFD simulations without phase change for the same geometry, initial and boundary conditions.

Figs. 5-7 show good agreement between the CFD- and PECM-predicted temperature patterns, solidification/melting contours, and pool centerline temperature profiles. However, the CFD phase-change simulation predicts

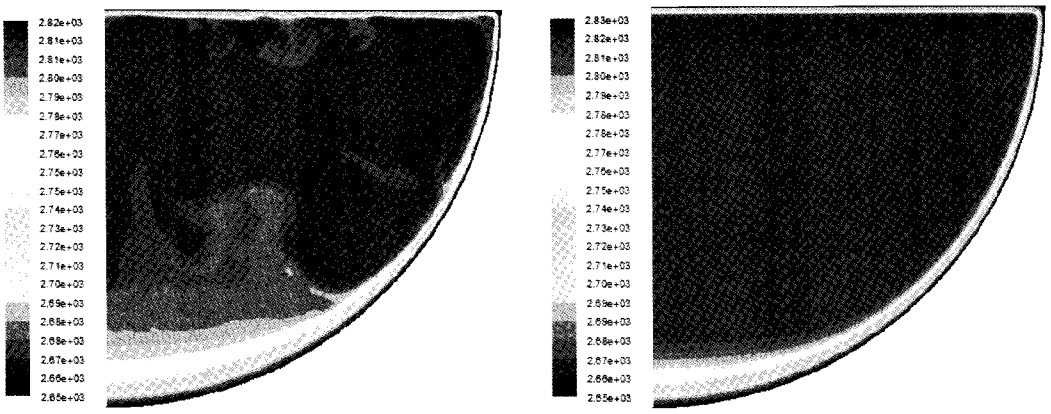

Fig. 5. CFD and PECM Simulation Temperature Contours, Color Bar Shows the Temperature (the Left Figure is CFD, the Right is PECM)

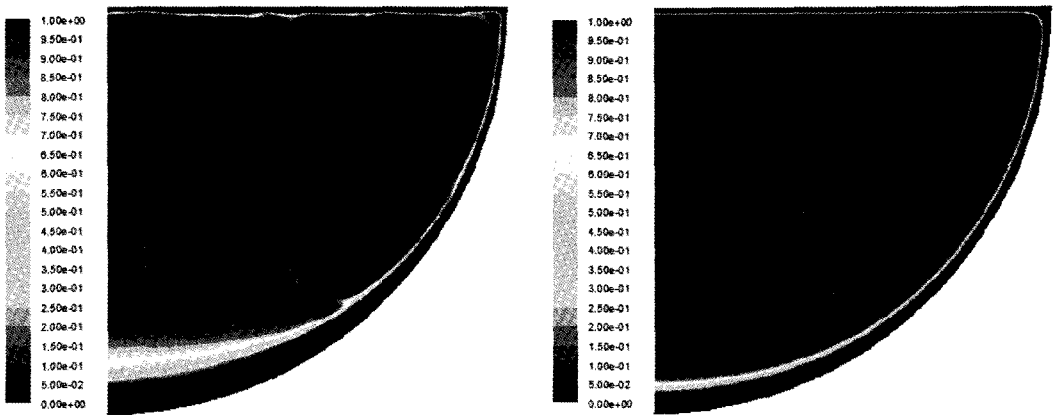

Fig. 6. Formation of Crusts along Cooled Boundaries, Color Bar Shows the Liquid Fraction (the Left Figure is CFD, the Right is PECM)

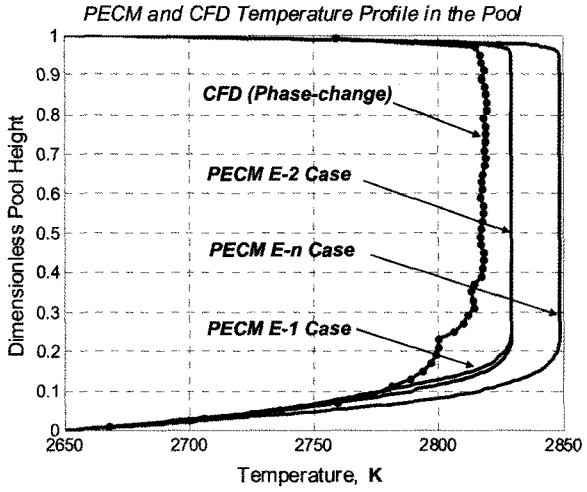

Fig. 7. CFD and PECM Simulation Pool Centerline Temperature Profiles

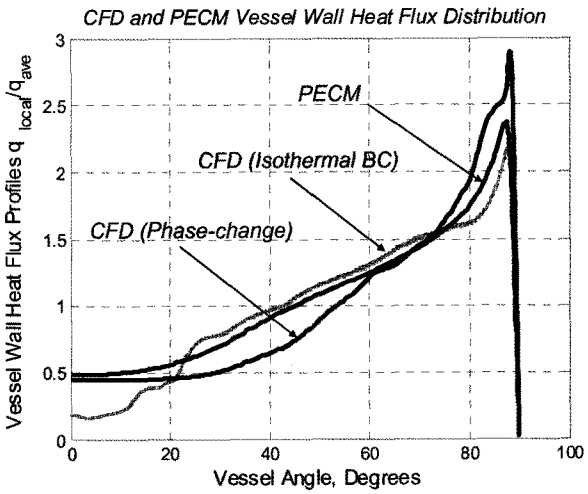

Fig. 8. Vessel Wall Heat Flux Profiles

lower bulk temperature than that of the PECM (Fig. 7). The CFD- and PECM-predicted downward heat flux profiles are similar in shape and value (Fig. 8). However, a slight discrepancy in the pool temperatures predicted by the CFD and PECM is observed (Table 2). The CFD simulation with phase change shows the lowest temperature of the pool. Among the mushy characteristic velocity models, the E-n model predicts the highest temperature of the pool. This means that the mushy characteristic velocity intensifies heat transport of the pool.

To analyze energy splitting of the pool, it is worth noting that for the PWR lower plenum geometry, the downward heat transfer coefficient, i.e. to the vessel wall, is not a simple summary of the sideward and downward heat transfer coefficients. To relate the upward and downward heat fluxes of a semi-spherical melt pool, it is necessary to apply a common heat transfer coefficient correlation for the vessel wall. We use the methodology suggested by Theofanous et al. [33], i.e. Steinberner-Reineke correlation for the upward heat flux:

$$Nu_{up} = 0.345 \times Ra^{0.233} \tag{16}$$

and Mayinger et al. correlation for the average downward heat flux, i.e. along the vessel wall:

$$Nu_{down} = 0.55 \times Ra^{0.2} \tag{17}$$

The calculated results (Table 2) show that the CFD results, the PECM results and the correlations agree within 25%.

In the remained parts of the paper, the linear dependency model of mushy characteristic velocity (model E-1) is applied. The PECM validation against the phase-change experiment is presented in the next subsection.

3.3 SIMECO Experiment

The SIMECO experiments were conducted in a slice-type facility (Fig. 9) which includes a semicircular section and a vertical section [12]. The diameter, height and width of the test section are 620x530x90 mm. Binary salt mixtures were employed as a melt simulant, both eutectic (50%-50%) and non-eutectic (20%-80%) mixtures of KNO_3-$NaNO_3$ were used. For the PECM validation we use the experiment with a eutectic mixture (the experiment number

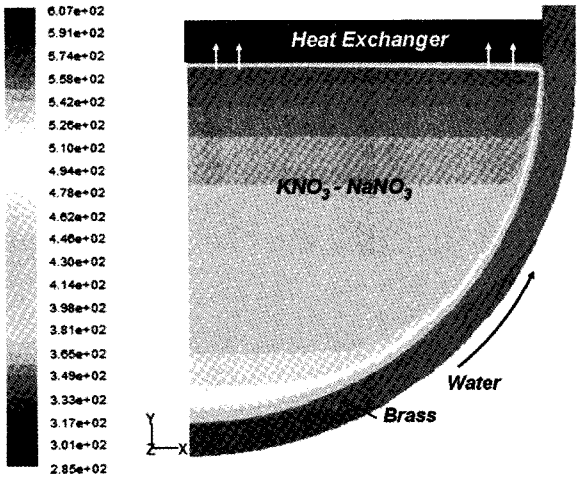

Fig. 9. SIMECO Experiment, Temperature Contour (in K, of the Middle Plane)

Table 2. Comparison of Energy Splitting (Upward and Downward Heat Fluxes) in the CFD and PECM Simulations for a Scaled PWR Lower Plenum

Cases	q_{up}, W/m^2	q_{down}, W/m^2	Superheat, K (T-T_{MP})	H_{pool}, m	q_{up} / q_{down}	Nu_{up}/Nu_{down}, equations (16) and (17)
CFD simulation (without phase change)	116046	76366	50.1	0.2	1.52	1.52
CFD simulation (with phase change)	118115	70120	43.4	0.1468	1.68	1.45
PECM simulation, mushy characteristic velocity **E-1**	124516	67019	51.5	0.1703	1.86	1.49
PECM simulation, mushy characteristic velocity **E-2**	125024	69988	51.7	0.1728	1.79	1.49
PECM simulation, no mushy velocity **E-n**	128557	67780	68.1	0.1798	1.89	1.50

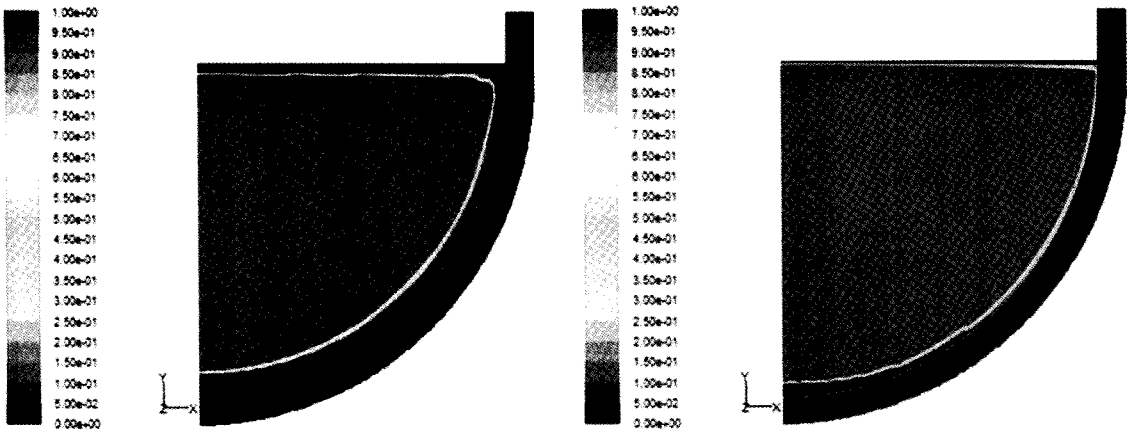

Fig. 10. SIMECO Experiment, Pool Formation after 0.83h and the Steady State (Liquid Fraction is Shown)

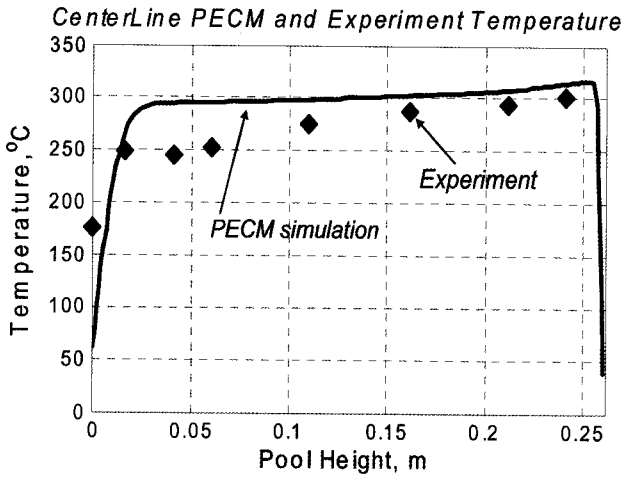

Fig. 11. Temperature Profile along the Pool Centerline: PECM vs. Experiment

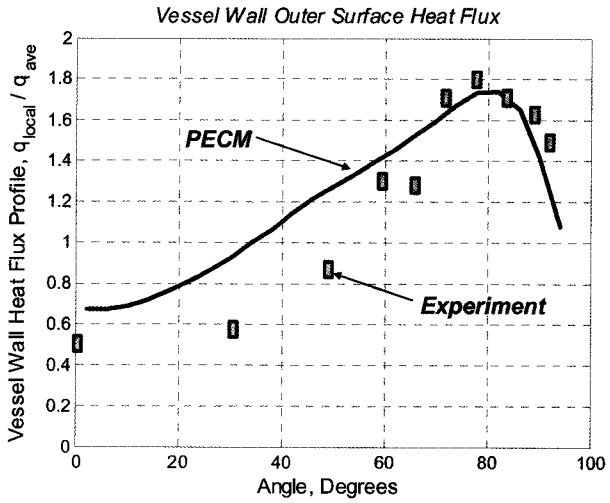

Fig. 13. Vessel Wall Heat Flux Distribution (PECM vs. Experiment)

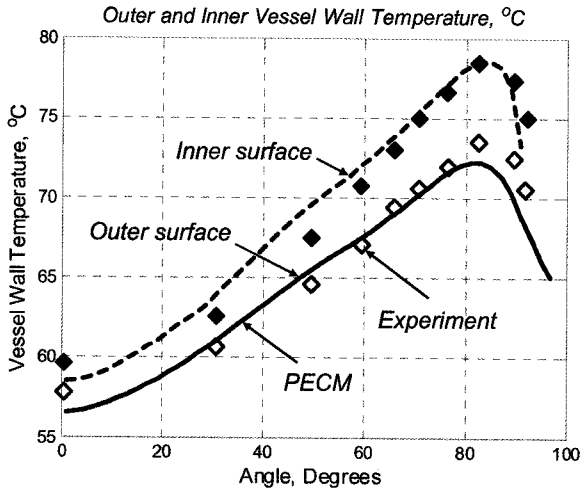

Fig. 12. Temperature Profiles of the Vessel Wall Inner and Outer Surfaces

is SSEu-10). We show that the PECM is able to simulate the melt pool with a eutectic material.

The following boundary conditions were used: the pool top surface is cooled by heat exchangers so isothermal boundary condition is applied; the angular brass surface is cooled by water coming from the lower part that suggests use of convection heat transfer boundary condition; the back wall is insulated, and the front wall is made of a special glass for visualization so a small heat flux, about 10-20 W/m^2 is applied for this wall. The initial temperature is 300 K.

Dynamics of pool formation and crust thickness can be seen in Fig. 10. Fair agreement of the PECM predicted results and the experimental data was obtained: the vertical temperature profiles are shown in Fig. 11; the vessel wall inner and outer surface temperature profiles are shown in Fig. 12; and the vessel wall heat flux distributions are shown in Fig. 13.

Slightly higher temperature along the vertical centerline is observed in the PECM simulation, and in the lower region of the pool, the predicted vessel wall heat flux is higher than that of the experiment. The increase in the PECM pool temperature compared with the experiment may be due to a heat loss during the experiment. The increase in the predicted vessel wall heat flux may result from a thinner crust thickness compared with the experimental in the pool's lowermost region. This larger experimental crust thickness may be explained by two possible reasons: first, more cold liquid accumulates in the lower region having flow from the upper inclined surfaces, and, second, the effect of non-uniformly volumetric heating of the experiment (electrically heated rods) compared with the uniformly volumetric heating of the PECM simulation that causes the cold liquid accumulated in the lowermost region to solidify.

3.4 Performance of the PECM

Due to its formulation, the PECM simulation allows larger time steps and coarser meshes compared to those of CFD simulations. More importantly, solving only the energy conservation equation without instantaneous fluid velocity (similarly to a conduction equation), the PECM effectiveness is obtained by a much lower number of iterations needed to achieve solution convergence in each

time step. A comparison of the CFD and PECM computing times is expressed in Table 3 for two transient phase-change scenarios presented in the previous subsections. The PECM simulations are 100-200 times faster than the corresponding CFD simulations.

4. APPLICATION OF THE PECM SIMULATION TOOL

4.1 Melt Pool Formation in a BWR Lower Head

In a previous study [2], we examined the potential of using CRGT coolant flows in the BWR lower head to remove the decay heat and retain the debris and corium

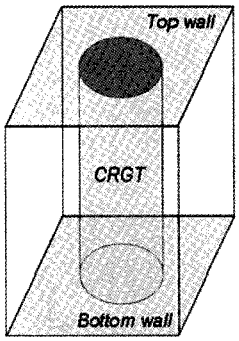

Fig. 14. Unit Volume in the BWR Lower Head ($312.6 \times 312.6 \times 400mm$)

Table 3. Comparison of CFD and PECM Calculation Times

Cases	CFD time step (seconds)	CFD calculation time (hours)	PECM time step (seconds)	PECM calculation time (hours)
Fluid layer cooled from the top	0.025	1224	0.5	10
Scaled PWR lower plenum	0.010	1560	0.2	8

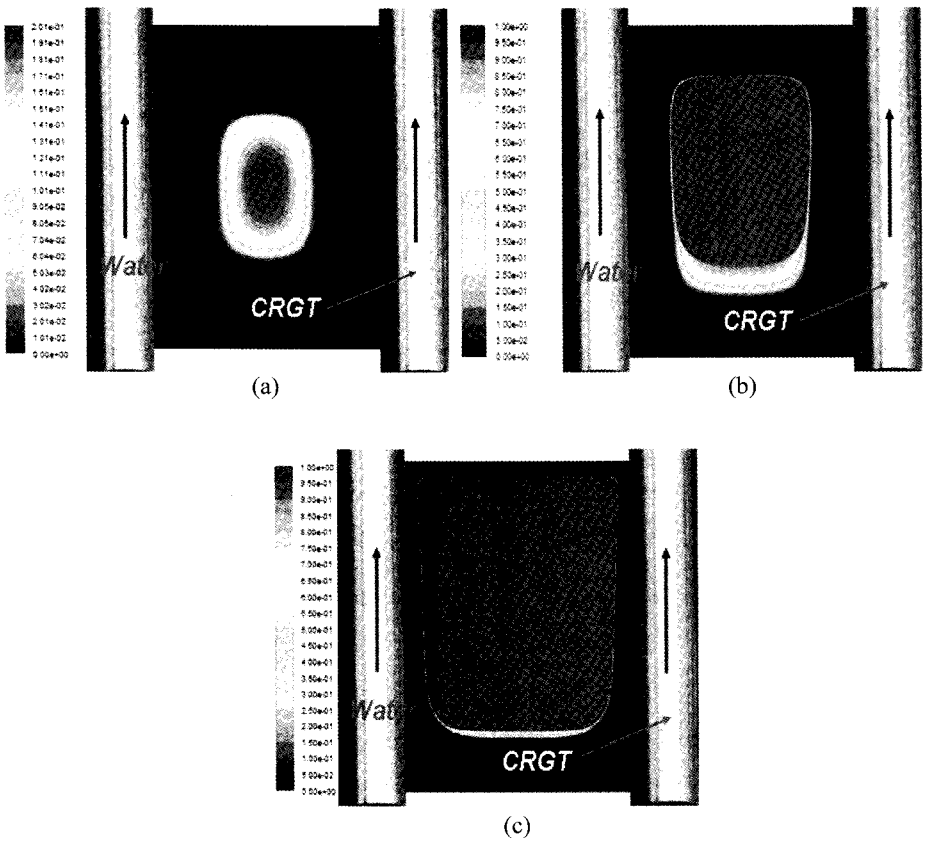

Fig. 15. Side View of the Formation of a Melt Pool in a Unit Volume Predicted by the 3D PECM Simulation: (a) Time $t = 2.7h$; (b) Time $t = 3.6h$; (c) Steady State, $t > 8.3h$. Color Bar Represents the Corium Liquid Fraction

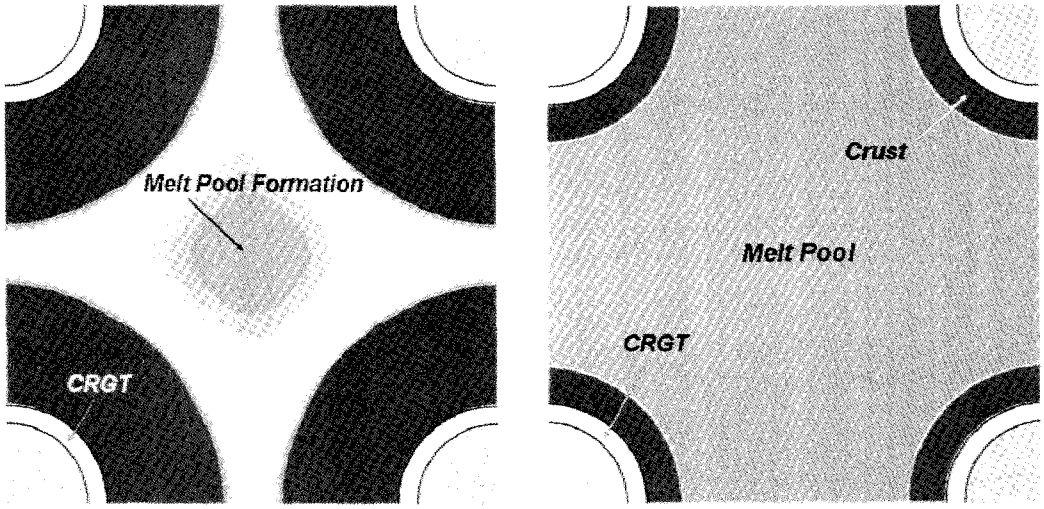

Fig. 16. Top View of the Formation of a Melt Pool in the Midst of Four CRGTs: (a) Formation Process; (b) Steady State

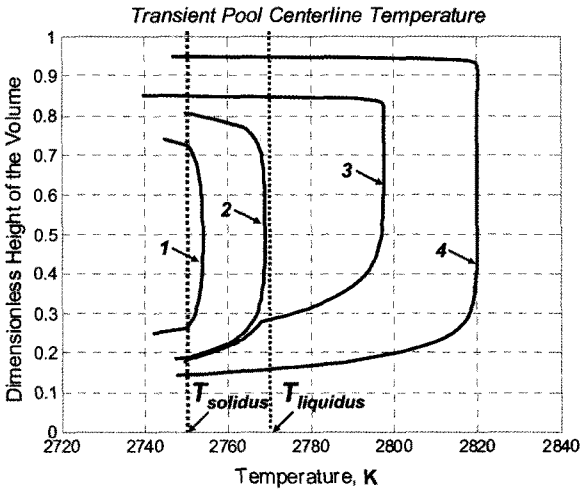

Fig. 17. Transient Pool Centerline Temperature Profiles: (1) $t=2.7h$; (2) $t=3.3h$; (3) $t=3.6h$; (4) $t>8.3h$

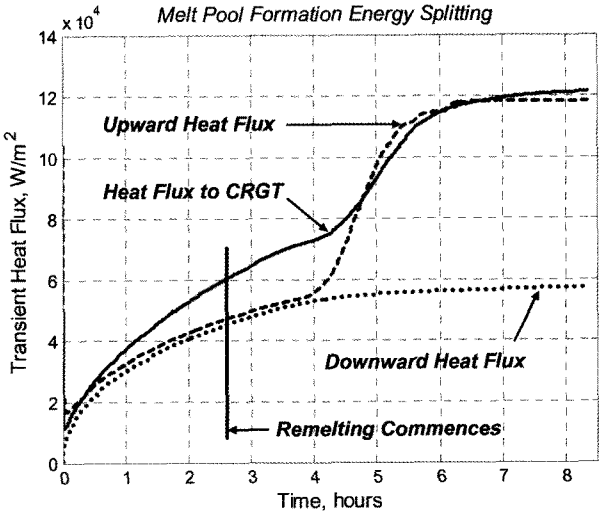

Fig. 18. Transient Heat Fluxes at the Computational Domain Boundaries

melt within the RPV. The presence of CRGTs significantly complicates the analysis of debris bed (cake), pool heat transfer, and consequently quantification of thermal loads imposed on the vessel structures, vessel failure mode and timing.

In this section, we apply the PECM to compute the dynamics of melt pool formation in a BWR unit volume. The unit volume is a 400 mm-height rectangular box surrounding one CRGT and filled with the decay-heated debris cake (Fig. 14). The objective of this simulation is to examine performance of the PECM in the BWR geometry and obtain new insights into the dynamics of the melt pool formation, energy splitting and thermal loadings on BWR vessel structures.

For the study case, the following assumptions are applied. The debris cake and the resulting melt pool are assumed to be homogeneous, with the volumetric decay

heat generation rate of 1 MW/m^3. The thermal conductivities of the debris cake and molten corium are 1 W/(m.K) and 3 W/(m.K), respectively. The debris cake initial temperature is 500 K. Isothermal boundary conditions (383 K, 450 K and 500 K) are applied to the computational domain's top, side and bottom boundaries.

As expected, the PECM depicts initiation of a melt pool in the midst of CRGTs (Fig. 15 and 16). The pool expands with time, both radially and axially, and becomes connected, forming a large melt pool surrounded by crust along the CRGT and vessel cooled walls. Remarkably, due to the isothermal boundary condition (500 K) applied to the bottom boundary and a low downward heat flux from the pool, a thick crust layer remains in the lowermost region. Fig. 17 shows temperature evolution of the debris cake and the pool at the centerline. Fig. 18 shows evolution of heat fluxes measured at the computational domain boundaries. It is seen that the debris cake starts to melt in 2.6 hours and a steady state is reached after 8.3 hours. The level of heat flux is quite modest. Fig. 19 shows the heat flux distribution along the CRGT, with a peaking factor of less than two and the maximum heat flux less than 200 kW/m^2.

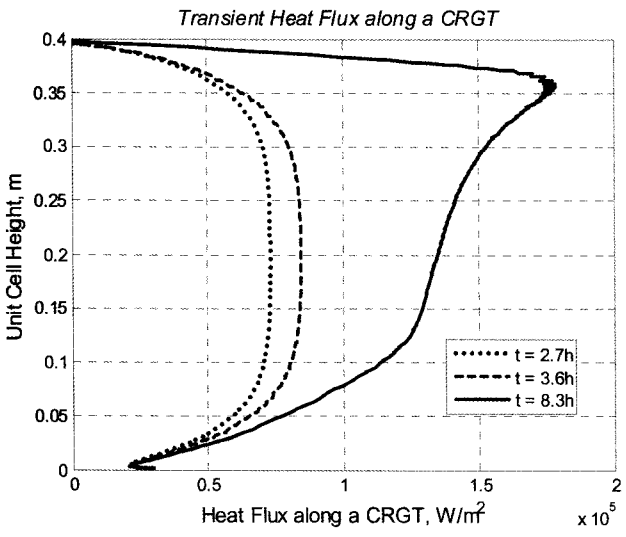

Fig. 19. Transient Heat Flux Distribution along a CRGT

Table 4 shows the pool superheat and energy splitting of the computational domain. For comparison, we also include results of the CFD simulation performed and presented in our previous paper [2] for the unit volume geometry. It is instructive to note that the CFD simulation was made without phase change, and the crust melting point (isothermal condition) was applied to all boundaries. We found that the PECM and the CFD simulations are consistent. Some differences are easily explained. The larger downward heat flux (measured at the domain bottom boundary) obtained in the PECM simulation is due to the energy contribution of a thick bottom crust. In the CFD simulation (without phase change), the superheat (61 K) can be determined relative to the melting point, e.g. the midpoint T_{MP} between solidus T_{SOL} and liquidus T_{LIQ}. In the PECM simulation, the determined superheat relative to the corium liquidus point is 50 K or adjusted to the melting point T_{MP} is 60 K.

4.2 Modeling and Scenario Uncertainties

The example of PECM-based simulation of heat transfer in a debris cake and melt pool formed in the lower head was made using several assumptions about the thermal condition at the boundaries of the computational domain and about effective physical properties (e.g. thermal conductivity, thermal expansion) of the cake materials, the molten corium and the mushy zone. We also assumed that Instrumentation Guide Tubes (IGTs) present in the BWR lower head do not significantly affect the heat transfer in a unit volume. Furthermore, the IGTs are plugged by either metallic or oxidic materials, thus inhibiting melt release from the RPV through the failed IGTs. In future, the analysis of the BWR lower head will include the RPV (as was done for the PWR case), where thermal boundary conditions (e.g. cooling from the RPV external wall) can be specified robustly and rather accident-scenario-independent.

Uncertainties in corium properties (in liquid, mushy, solid and porous states) can be reduced with the availability of corresponding data. However, given the value range of relevant properties, the significance of their uncertainties is judged to be far less important than uncertainties in an

Table 4. Energy Splitting and Superheat of the Pool

Simulation tool	Superheat of the pool, K	Upward heat flux q_{up}, W/m^2	Sideward heat flux q_{sd}, W/m^2	Downward heat flux q_{down}, W/m^2
PECM	50	118339	121419	57217
CFD [2] without phase change	61.1	169649	108267	29581

accident scenario. In fact, it should also be noted that the case presented considers a highly simplified configuration of core melt in the lower plenum, namely transformation of a homogeneous debris cake into a homogeneous melt pool. Accident sequences in LWR are expected to involve stratified cakes and melt pools, where material and decay heat distributions are heterogeneous, spatially dependent and evolving in time. While the PECM method developed in this paper allows one to account for such heterogeneities in the analysis of heat transfer in the lower plenum, scenarios of melt relocation must be provided as input data. We envision that the PECM-based mechanistic simulation is coupled with a severe accident system code (e.g. MELCOR) to leverage on the strength of the two methods.

5. CONCLUDING REMARKS

We have extended the Effective Convectivity Model (ECM) to phase-change problems (Phase-change ECM or PECM) and performed the PECM validation by a dual approach. We recommend using the linear dependency of the heat transfer characteristic velocity in a mushy zone on the liquid fraction in the PECM for simulations of the binary melt phase-change dynamics. The PECM has proved to be suitable and effective as a tool for simulations of core melt pool formation in complex geometry such as in a BWR lower plenum during hypothetical severe accident scenarios. In our future studies we plan to use the PECM to perform analyses of transient processes of core melt pool formation in a BWR lower head with and without coolant flow in CRGTs. The PECM can be further extended to include a metallic layer to analyze heat transfer of a stratified melt pool, to study the focusing effect and reactor pressure vessel ablation. The PECM can be coupled with a structural mechanics model [34] to study the reactor pressure vessel's thermo-mechanical response, creep, and failure.

NOMENCLATURE

Arabic

C_p	Specific heat capacity, J/kg.K
F_L	Liquid fraction
F_S	Solid fraction
g	Gravitational acceleration, m/s^2
H	Enthalpy, J/kg
H_{pool}, W_{pool}	Height, width of a volume or melt pool or fluid layer, m
h	Sensible heat, J/kg
k	Conductivity, W/m.K
L	Latent heat of phase change, J/kg
Nu	Nusselt number, $Nu = \frac{qH_{pool}}{k\Delta T}$
Pr	Prandtl number, $\Pr = \nu/\alpha$
q	Heat flux, W/m^2
Q_v	Volumetric heat source, W/m^3
Ra	Rayleigh number (internal), $Ra = \frac{g\beta Q_v H_{pool}^5}{k\nu\alpha}$
Ra_y	Local Rayleigh number, $Ra_y = \frac{g\beta\Delta T y^3}{\nu\alpha}$
S_c	Modified source term, W/m^3
t	Time, s
T	Temperature, K
u	Fluid velocity, m/s
U	Characteristic velocity, m/s
y	Local vertical coordinate, m

Greek

α	Thermal diffusivity, m^2/s, $\alpha = \frac{k}{\rho.C_p}$
β	Thermal expansion coefficient, 1/K
λ	Porosity
ΔH	Latent heat of fusion, J/kg
ΔT	Temperature difference, K
ρ	Density, kg/m^3
ν	Kinematics viscosity, m^2/s
μ	Dynamic viscosity, Pa.s

Subscripts and superscripts

BC	Boundary condition
cond	Conduction
down	Downward
L	Liquid
LIQ	Liquidus
MP	Middle point
mushy	Mushy
side	Sideward
REF	Reference
SOL	Solidus
up	Upward

ACKNOWLEDGMENTS

The authors thank Dr. W. Frid, Dr. P. Kudinov and Professor B.R. Sehgal for stimulating discussions and helpful comments. The support from the Swedish Nuclear Power Inspectorate SKI, Swedish power companies, European Commission, Nordic Nuclear Safety Program NKS and Switzerland's Nuclear Safety Commission HSK under the APRI, SARNET and MSWI programs is gratefully acknowledged.

REFERENCES

[1] B. R. SEHGAL, V. A. BUI, T. N. DINH and R. R. NOURGALIEV, "Heat Transfer Process in Reactor Vessel Lower Plenum during A Late Phase of In-Vessel Core Melt Progression", *J. Advances in Nuclear Science and Technology*, **Vol. 26**, pp. 103-135, 1998.

[2] C. T. TRAN, T. N. DINH, "Analysis of Melt Pool Heat Transfer in a BWR Lower Head", *Transactions of ANS*

Winter Meeting, Albuquerque, NM, USA, November 12-18, Vol. 95, pp. 629-631, 2006.

[3] "MAAP4 Users Manual", *Fauske Associated Inc.*, Vol. 2, 1999.

[4] R. O. GAUNTT et al., "MELCOR Computer Code Manual, Core (COR) Package Reference Manuals", *NUREG/CR-6119, Vol. 2, Rev.2*, Version 1.8.6, September 2005.

[5] C. T. TRAN, T. N. DINH, "An Effective Convectivity Model for Simulation of In-Vessel Core Melt Progression in Boiling Water Reactor", *2007 International Congress on Advances in Nuclear Power Plants (ICAPP 2007)*, Nice Acropolis, France, May 13-18, 2007.

[6] V. A. BUI and T. N. DINH, "Modeling of Heat Transfer in Heated-Generating Liquid Pools by an Effective Diffusivity-Convectivity Approach", *Proceedings of 2nd European Thermal-Sciences Conference*, Rome, Italy, pp.1365-1372, 1996.

[7] F. B. CHEUNG , S.W. SHIAH, D.H. CHO and M.J. TAN, "Modeling of Heat Transfer in A Horizontal Heat-Generating Layer by An Effective Diffusivity Approach". *ASME HTD-***Vol. 192**, pp.55-62, 1992.

[8] UDF Manual, **Fluent** *6.2 Documentation*, Fluent Inc. 2005.

[9] V. ASMOLOV, N. N. PONOMAREV-STEPNOY, V. STRIZHOV, B. R. SEHGAL, "Challenges Left in the Area of In-Vessel Melt Retention", *J. Nuclear Engineering and Design*, **Vol. 209**, pp. 87-96, 2001.

[10] V. G. ASMOLOV, S. V. BECHTA, V. B. KHABENSKY et al., "Partitioning of U, Zr and Fe between Molten Oxidic and Metallic Corium", *Proceeding of MASCA Seminar 2004*, Aix-en-Provence, France, 2004.

[11] V. STRIZHOV, V. ASMOLOV, "Major Outcomes of the RASPLAV Project", *RASPLAV Seminar 2000*, Munich, November, 2000.

[12] B. R. SEHGAL, V. A. BUI, T. N. DINH, J. A. GREEN, G. KOLB, "SIMECO Experiments on In-Vessel Melt Pool Formation and Heat Transfer with and without a Metallic Layer", *Proceedings of In-Vessel Core Debris Retention and Coolability Workshop*, Garching, Germany, March 3-6, pp. 205-213, 1998.

[13] A. MIASSOEDOV, T. CRON, J. FIOT, S. SCHMIDT-STIEFEL, T. WENZ, I. IVANOV, D. POPOV, "Results of the LIVE-L1 Experiment on Melt Behavior in RPV Lower Head Performed within the LACOMERA Project at the Forschungszentrum Karlsruhe", *Proceedings of 15th International Conference on Nuclear Engineering Nagoya (ICONE)*, Japan, April 22-26, 2007.

[14] M. HELLE, O. KYMALAINEN and H. TUOMISTO, "Experimental Data on Heat Flux Distribution from a Volumetrically Heated Pool with Frozen Boundaries", *Proceedings of In-Vessel Core Debris Retention and Coolability Workshop*, Garching, Germany, March 3-6, pp. 173-183, 1998.

[15] L. BERNAZ, J.- M. BONNET, B. SPINDLER, C. VILLERMAUX, "Thermal Hydraulic Phenomena in Corium Pools: Numerical Simulation with TOLBIAC and Experimental Validation with BALI", *Proceedings of In-Vessel Core Debris Retention and Coolability Workshop*, Garching, Germany, March 3-6, pp. 185-193, 1998.

[16] M. OKADA, "Analysis of Heat Transfer during Melting from a Vertical Walls", *Int. J. Heat Mass Transfer*, **Vol. 27 (11)**, pp. 2057-2066, 1984.

[17] C. J. HO and S. CHEN, "Numerical Simulation of Melting of Ice around a Horizontal Cylinder", *Int. J. Heat Mass Transfer*, **Vol. 29 (9)**, pp. 1359-1368, 1986.

[18] N. SHAMSUNDAR, E. M. SPARROW, "Analysis of Multidimensional Conduction Phase change Via the Enthalpy Model", *J. Heat Transfer*, **Vol. 97 (3)**, pp. 333-340, 1975.

[19] V. R. VOLLER and C. PRAKASH, "A Fixed Grid Numerical Modelling Methodology for Convection-Diffusion Mushy Region Phase-Change Problems", *J. Heat Mass Transfer*, **Vol. 30 (8)**, pp.1709-1719, 1987.

[20] Y. CAO, A. FAGHRI and W. S. CHANG, "A Numerical Analysis of Stefan Problems for Generalized Multi-Dimensional Phase-Change Structures Using the Enthalpy Transforming Model", *Int. J. Heat Mass Transfer*, **Vol. 32 (7)**, pp. 1289-1298, 1989.

[21] P. J. PRESCOTT, F. P. INCROPERA, D. R. GASKELL, "Convective-Transport Phenomena and Macrosegregation during Solidification of a Binary Metal Alloy. 2. Experiments and Comparisons with Numerical Predictions", *J. Heat Transfer-Transactions of the ASME*, **Vol. 116 (3)**, pp. 742-749, Aug. 1994.

[22] B. BINET, M. LACROIX, "Numerical Study of Natural-Convection-Dominated Melting inside Uniformly and Discretely Heated Rectangular Cavities", *Numerical Heat Transfer Part A-Applications*, **Vol. 33 (2)**, pp. 207-224, 1998.

[23] V. R. VOLLER and A. D. BRENT, "Modelling the Mushy Region in a Binary Alloy", *App. Math Modelling*, **Vol. 14**, pp. 320-326, 1990.

[24] T. W. CLYNE, "Numerical Modeling of Directional Solidification of Metallic Alloys", *J. Metal Science*, **Vol. 16 (9)**, pp. 441-450, 1982.

[25] V. R. VOLLER and C. R. SWAMINATHAN, "General Source-Based Method for Solidification Phase Change", *J. Numerical Heat Transfer, Part B*, **Vol. 19**, pp. 175-189, 1991.

[26] U. STEINBERNER and H.H. REINEKE, "Turbulent Buoyancy Convection Heat Transfer with Internal Heat Sources". *Proceedings of the 6th Int. Heat Transfer Conference*, Toronto, Canada, Vol.2, pp.305-310, 1978.

[27] O. KYMALAINEN, H. TUOMISTO, T. G. THEOFANOUS, "In-Vessel Retention of Corium at the Loviisa Plant", *J. Nuclear Engineering and Design*, **Vol. 169**, pp. 109-130, 1997.

[28] T. G. THEOFANOUS, M. MAGUIRE, S. ANGELINI, T. SALMASSI, "The First Results from the ACOPO Experiment", *J. Nuclear Engineering and Design*, **Vol. 169**, pp.49-57, 1997.

[29] T. C. CHAWLA and S. H. CHAN, "Heat Transfer From Vertical/Inclined Boundaries of Heat-Generating Boiling Pools", *J. Heat Transfer*, **Vol. 104**, pp.465-473, 1982.

[30] M. RAMACCIOTTI, C. JOURNEAU, F. SUDREAU, G. COGNET, "Viscosity Models for Corium Melts", *J. Nuclear Engineering and Design*, **Vol. 204**, pp. 377-389, 2001.

[31] F. A. KULACKI and A. A. EMARA, "Steady and Transient Thermal Convection in a Fluid Layer with Uniform Volumetric Energy Sources", *J. Fluid Mech.*, **Vol. 83**, part 2, pp.375-395, 1977.

[32] R. R. NOURGALIEV, T. N. DINH, "The Investigation of Turbulence Characteristics in an Internally-Heated Unstably-Stratified Fluid Layer", *J. Nuclear Engineering and Design*, **Vol. 178**, pp. 235-258, 1997.

[33] T. G. THEOFANOUS, C. LIU, S. ADDITON, S. ANGELINI, O. KYMALAINEN, T. SALMASSI, "In-vessel Coolability

and Retention of a Core Melt", *DOE/ID-1046*, November 1994.

[34] H.-G. WILLSCHUETZ, E. ALTSTADT, B. R. SEHGAL, F.-P. WEISS, "Recursively Coupled Thermal and Mechanical FEM - Analysis of Lower Plenum Creep Failure Experiments", *Annals of Nuclear Energy*, **Vol. 33**, pp.126-148, 2006.